Proceedings of the 14th International Heat Transfer Conference
IHTC 14
August 8-13, 2010, Washington D.C., USA

IHTC14-23053

SIMULATION OF CHAR DUST COMBUSTION INSIDE A PYROSCRUBBER DOWNSTREAM OF A PETROLEUM COKE CALCINING KILN

Lei Zhao and Ting Wang
Energy Conversion and Conservation Center
University of New Orleans
New Orleans, LA 70148-2220, USA

ABSTRACT

A pyroscrubber is a furnace used in the petroleum coke calcining industry to recover energy from the carbonaceous contents, including char dust and hydrocarbon volatiles of the exhaust gas from the calcination kiln. The combusted hot gases are used to generate steam and produce electricity, so it is important to optimize the pyroscrubber performance to produce high-grade combusted gases to generate steam but with minimal emissions.

A previous study employed the locally-homogeneous flow (LHF) model to study rhe means to improve combustion efficiency and reduce emissions. In the LHF model, the inter-phase exchange rates of mass, momentum and energy are assumed to be infinitely fast, so the dispersed phase (char dust) can be simplified as the gas phase, and the complex two-phase flow is then treated as a single-phase flow. In this study, LHF model is replaced with a solid particle combustion model by incorporating both finite-rate heterogeneous and homogeneous combustion processes. Results reveal that the particle combustion model generates much higher local flame temperature (2200K) than in LHF model (1800K). All char particles are burned before or in the high-bay area. Total energy output of the case with particle combustion model is 92% of the LHF model. Furthermore, motivated by the potential energy saving from removing the air blower power supply, this study further investigates the possible benefit of running the pyroscrubber with the ventilation doors open. Three cases with different combinations of air injections and door opening have been studied. Results show that the gas flow is stably stratified with a large amount of the entrained cold air moving at the bottom of the chamber and the hot combusted gas moving through the top. With bottom doors completely open, sufficient air can be drawn into the pyroscrubber without the need of blowing air in, but the combustion gases will be overcooled making this practice unfavorable from the energy saving point of view.

INTRODUCTION

Petroleum coke (petcoke) is usually calcined in a gas-fired rotary kiln or rotary hearth at high temperatures, around 1,200 to 1,350°C (2,192 to 2,462°F), to remove moisture, drive off volatile matters, increase the density of the coke structure, increase physical strength, and increase the electrical conductivity of the material. The product is hard, dense carbon (calcined petcoke) with low hydrogen content and good electrical conductivity. These properties along with the low metals and ash contents make calcined petcoke the best material currently available for making carbon anodes for smelting of alumina to aluminum [1]. An extensive discussion of various properties of green and calcined petroleum cokes for aluminum anode grade carbon production can be found in the study of Lee et al. [2].

A pyroscrubber is namely a furnace burning carbon particles in a stream of waste gases, particularly from a petcoke calcination kiln or hearth. The schematic of the calcining process for petcoke is shown in Fig. 1. The combusted hot gases from the pyroscrubber are ducted through a boiler to produce steam that is used to generate electricity through steam turbines. A pyroscrubber typically comprises of a U-shaped combustion chamber having a first passage arranged parallel with (preferably above) a second passage, so there is a reversal in gas flow direction between the two passages. The main function of the pyroscrubber is to oxidize the carbonaceous contents, including hydrocarbon volatiles in the exhaust gas from the calcination kiln, and recover energy from the waste stream and leave no more than small traces of unburned volatiles, solid carbon, ashes, or emissions (e.g. CO, NO_x and SO_x) in the flue gas finally discharged [3]. Since the hot gases exhausted from the pyroscrubber are used to generate steam and produce electricity, it is essential to keep the energy quality of the gases high (ie. at high temperature) but with low emissions.

Control of NO_x emission is one of the major considerations in the design of a pyroscrubber. NO_x emissions cause serious health issues, ranging from bronchitis to altered immune system function. NOx also contributes significantly to environmental problems such as acid rain and ozone depletion. NO_x emission consists of mostly nitric oxide (NO). It also contains nitrogen oxide (NO_2) and nitrous oxide (N_2O). The quantity of NO_x formed depends on the three T's: Temperature, Time, and Turbulence. NO_x control technologies currently used within the industry can be grouped into two categories i.e. combustion modifications and

post-combustion NO_x control technologies. The first addresses reduced production of NO_x by making changes in the combustion process or the fuel stream. The second involves mitigating the NO_x that has been produced by the application of post-combustion technology through the use of chemical reagents. A strategy to reduce NO_x emission for a pyroscrubber has been studied by Zhao and Wang [4] by implementing a multi-stage combustion pattern.

Sulfur content in the petcoke has to be removed in order to be directly utilized in the fabrication of carbon products. Thermal desulfurization process is typically implemented in the calcining kiln by heating up the coke from 500°C (932 °F) to 1500 °C (2,732 °F) depending on different calcination stages and sulfur content requirement. The desulfurization process can be applied using sorbent injection, dry flue gas desulfurization or wet flue gas desulfurization via a scrubber.

Pyroscrubbers of different designs have been employed worldwide to compete for more efficient and cleaner combustion of exhaust gases from coke calcination kilns or hearths. But very limited literature can be found about pyroscrubber design and studies from public resources. Zhao and Wang [4] studied means to improve pyroscrubber combustion efficiency and reduce emissions through a numerical simulation inside a pyroscrubber employing the locally-homogeneous flow (LHF) model. In the LHF model, the inter-phase exchange rates of mass, momentum and energy are assumed to be infinitely fast, so the dispersed phase (char dust) can be simplified as the gas phase, and the complex two-phase flow is then treated as a single-phase flow which reduces the computational load significantly. The simulation results were compared with the plant measurement data and the comparison showed that the LHF model yields reasonable overall result (average temperature, energy output and NO_x emission) at the pyroscrubber outlet. But the computational convenience brought by the LHF model is at the cost of lacking particle combustion details and the LHF model is not expected to accurately describe the physical phenomena of carbon dusts combustion process.

In this study, LHF model is replaced with a solid particle combustion model by incorporating both finite-rate heterogeneous and homogeneous combustion processes, which provide a more accurate modeling of the complex solid carbon particle surface reaction, heat transfer, and species transport. Due to the complexity of dealing with random particle tracking and the heterogeneous combustion process, intensive computational power is expected. Stoichiometric air supply is studied and the results of the computational fluid dynamics (CFD) model are compared with the LHF results and the plant temperature measurement data

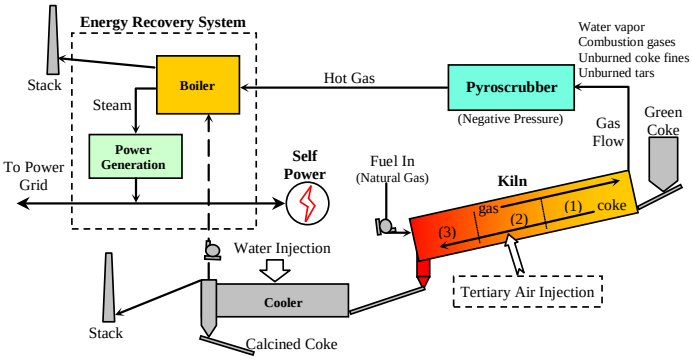

Fig. 1 Schematic of the calcining process for petroleum coke

Furthermore, motivated by the potential energy saving from cutting the air blower power supply for the pyroscrubber air injection, this study also investigates the condition of running the pyroscrubber with the ventilation doors on the bottom open. Three cases with different combinations of air injections and door opening are studied.

MODELING AND METHODOLOGY

The pyroscrubber investigated in this paper is shown in Figs. 2 and 3. Geometric information of the pyroscrubber is obtained through the blueprints of a calcination plant in Louisiana. The modeled domain includes part of the calcining kiln, settling chamber, inlet duct (which connects the settling chamber with the main chamber), air injection section, main chamber, and outlet duct, connecting the main chamber to the boiler. The main chamber is around 35 ft wide, 103 ft long and 40 ft tall. Details of the air injectors and the burner are shown in Fig. 3.

The inlet of the pyroscrubber receives exhaust gases from the exit of the calcining kiln. After completion of the calcining process inside the kiln, combustion product gases, together with unburned volatiles and coke fines are fed into the pyroscrubber through the settling chamber and the inlet duct. Air is injected into the main chamber through two air injection sections. The first air injection section consists of 28 air injection tubes shooting at 45° from the vertical direction (Y direction). The second air-injection section consisting of four burners is located on the east wall of the low-bay main chamber. They are used to inject natural gas during the start-up period and switched to blowing air into the main chamber after the ignition and start-up process complete. Hot product gases exit the pyroscrubber main chamber through the outlet duct and are fed into the steam boiler to generate electricity.

The major characteristics and general assumptions in this study are listed below:

1. The flow inside the pyroscrubber is three dimensional, incompressible, and turbulent.
2. Gas species involved in this study are Newtonian fluids with variable properties as functions of temperature.
3. Buoyancy and radiation effects are considered.
4. Non-slip and adiabatic wall conditions are assumed.

The CFD commercial software FLUENT (version 6.2.16) is used. The simulation utilizes the segregated solver, which employs an implicit pressure-correction scheme. The SIMPLE algorithm is used to couple the pressure and velocity. Second order upwind scheme is selected for spatial discretization of the convective terms and species. Converged results are obtained after the specified residuals are met. A converged result renders mass residual of 10^{-3}, energy residual of 10^{-5}, and momentum and turbulence kinetic energy residuals of 10^{-5}. These residuals are the summation of the imbalance for each cell, scaled by a representative of the flow rate. Typically, 8,000 to 12,000 iterations are needed to obtain a converged result, which takes about 40~60 hours on a 10-node computer cluster of parallel computation with each node a 2.8 GHz Pentium personal computer.

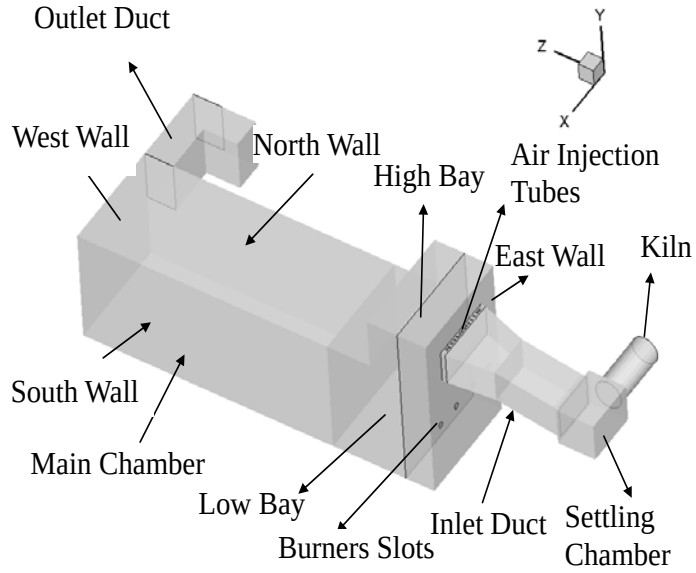

Fig. 2 A 3-D view of the pyroscrubber

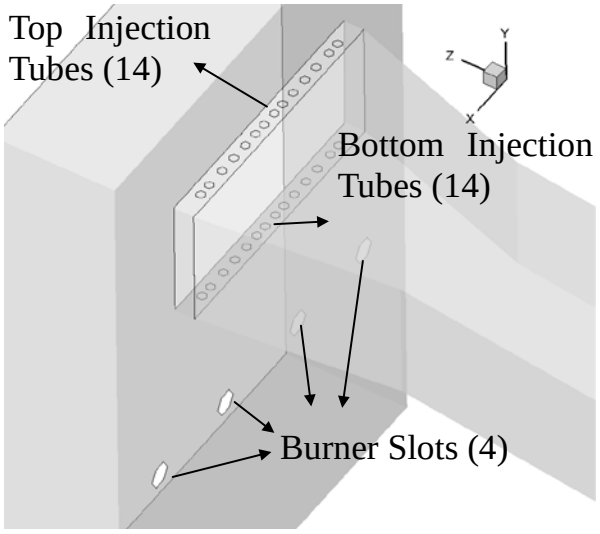

Fig. 3 Detailed layout of air injections and burners

Governing Equations

The general conservation equations for mass, momentum and energy in general forms are shown below.

$$\frac{\partial \rho}{\partial t} + \nabla \bullet (\rho \vec{v}) = 0 \tag{1}$$

$$\frac{\partial}{\partial t}(\rho \vec{v}) + \nabla \bullet (\rho \vec{v}\vec{v}) = -\nabla p + \nabla \bullet (\bar{\bar{\tau}}) + \rho \vec{g} + \vec{F} \tag{2}$$

$$\frac{\partial}{\partial t}(\rho e) + \nabla \bullet (\vec{v}(\rho e + p)) = \nabla \bullet \left(k_{eff} \nabla T - \sum_j h_j \vec{J}_j + (\bar{\bar{\tau}}_{eff} \bullet \vec{v}) \right) + S_h \tag{3}$$

In this study, the steady-state solution for the conservation equations is solved, so the transient terms in the equations are not included in the computation. The momentum equations are solved with the complete three-dimensional Navier-Stokes equations. The stress tensor $\bar{\bar{\tau}}$ is given by

$$\bar{\bar{\tau}} = \mu \left[\left(\nabla \vec{v} + \nabla \vec{v}^{\,T} \right) - \frac{2}{3} \nabla \bullet \vec{v} \bullet I \right] \tag{4}$$

where I is the unit tensor.

In the energy equation, e is given as

$$e = h - \frac{p}{\rho} + \frac{v^2}{2} \tag{5}$$

"h" is the sensible enthalpy and for incompressible flow and it is given as

$$h = \sum_j Y_j h_j + \frac{p}{\rho} \tag{6}$$

$$h_j = \int_{T_{ref}}^{T} c_{p,j} dT \tag{7}$$

T_{ref} is the reference temperature, taken as 298.15 K. S_h in the energy equation is the source term and is provided by the net enthalpy formation rates from the species transport reactions.

Inlet Condition

The composition of the pyroscrubber inlet species is complex due to the calcining and combustion process inside the kiln. The detailed process of inlet condition setup can be found in [4]. Some inlet conditions are from the studies of the rotary kiln in [5] and [6]. The species composition and feeding rate at the main inlet, air injection tubes and burner slots are summarized in Table 1. Other boundary conditions of different surfaces are listed below:

1. Inlet temperature:
   a. Main inlet gases: 500 K (440.33 °F).
   b. Air from the injection tubes: 300 K (80.33 °F)
   c. Air from the burner slots: 300 K (80.33 °F)

2. Pressure outlet -- The outlet is defined with the constant pressure. The pressure, temperature, and species mass fraction of the mixture of the potential reverse flow (if it occurs) are specified as follows:
   a. Gas outlet: Constant pressure outlet condition, P=1atm

b. Reversed flow temperature condition, T_{outlet} = 1000K (1340.33 °F)
c. Reversed flow mass fraction:O_2 = 0.23 and N_2= 0.77

3. Wall -- The walls are treated as adiabatic with no-slip velocity condition:

a. Adiabatic wall condition, heat flux = 0
b. No slip condition at the walls, u = 0, v = 0, w = 0

Table 1 Inlet species composition summary

inlet species	mass flow(kg/s)	mass fraction	stoichiometric air needed (kg/s)
N_2	9.070	0.622	0.000
CH_4	0.000	0.000	0.000
C	1.537	0.105	17.669
H_20	1.154	0.079	0.000
CO_2	2.159	0.148	0.000
O_2	0.237	0.016	(1.021)
volatiles	0.419	0.029	5.719
total	14.577	1.000	22.366
burner air	11.483	0.513	11.483
top air inject	5.442	0.243	5.442
bottom air inject	5.442	0.243	5.442

Dispersed-Phase Model (Carbon Particles)

Particle dynamics and heat transfer

Based on the Newton's 2nd Law, particle motion in the airflow can be formulated by

$$m_p d\mathbf{v_p}/dt = \sum \mathbf{F} \tag{8}$$

where m_p is the particle mass, and v_p is the particle velocity (vector). The right-hand side is the combined force acted on the particles, which normally includes the hydrodynamic drag, gravity and other forces such as the "virtual mass" force, thermophoretic force, Brownian force, and Saffman's lift force.

The radiation is included in the continuous phase between walls and gases, but radiation is not considered on the particle surface. Without considering the radiation heat transfer, the particle's heat transfer depending on convection and evaporation is given in the following equation.

$$m_p c_p \frac{dT}{dt} = \pi d^2 h(T_\infty - T) + \frac{dm_p}{dt} h_{fg} \tag{9}$$

where h_{fg} is the latent heat. The convective heat transfer coefficient (h) can be obtained with an empirical correlation [7-8]:

$$Nu_d = \frac{hd}{\lambda} = 2.0 + 0.6 Re_d^{0.5} Pr^{0.33} \tag{10}$$

where N_u is the Nusselt number, and P_r is the Prandtl number.

The mass change rate in Eq. (9) is governed by concentration difference between particle surface and the gas stream,

$$-\frac{dm_p}{dt} = \pi d^2 k_c (C_s - C_\infty) \tag{11}$$

where k_c is the mass transfer coefficient, and C_s is the vapor concentration at the particle surface. C_∞ is the vapor concentration of the bulk flow, obtained by solving the transport equations. The values of k_c can be given from a correlation similar to Eq. (10) by [9-10].

Stochastic particle tracking

The turbulence effect on particles dispersion is considered by using stochastic tracking. Basically, the particle trajectories are calculated by using the instantaneous flow velocity ($\bar{u} + u'$) rather than the average velocity ($\bar{u}$). The velocity fluctuations are then given as:

$$u' = \varsigma\left(\overline{u'^2}\right)^{0.5} = \varsigma(2k/3)^{0.5} \tag{12}$$

where ζ is a normally distributed random number [11]. This velocity will apply during the characteristic lifetime of the eddy (t_e), a time scale calculated from the turbulence kinetic energy and dissipation rate. After this time period, the instantaneous velocity will be updated with a new ζ value until a full trajectory is obtained

Particle Combustion Model

The particle combustion model involves two different types of reaction: homogeneous reaction and heterogeneous combustion. The details of the two types of reactions are explained in detail below.

Homogeneous reaction

The species transport equation in general form is given as:

$$\frac{\partial}{\partial t}(\rho Y_i) + \nabla \bullet (\rho \vec{v} Y_i) = -\nabla \bullet \vec{J}_i + R_i + S_i \tag{13}$$

where R_i is the net rate of production of species i by chemical reaction. S_i is the rate of creation (a source term) from the dispersed phase. $\bar{J}_i$ is the diffusion flux of species i, which arises due to concentration gradients. For turbulent flows, mass diffusion flux is given as

$$\bar{J}_i = -\left(\rho D_{i,m} + \frac{\mu_t}{Sc_t}\right)\nabla Y_i \tag{14}$$

where Sc_t is the turbulent Schmidt number given as $\mu_t/\rho D_t$, where μ_t is the turbulent viscosity and D_t is the turbulent diffusivity.

In the particle combustion case, finite-Rate/Eddy-Dissipation model is used to simulate the homogeneous reactions. Reaction rate based on the Laminar Finite-Rate Model and Eddy-Dissipation Model are calculated and compared. The minimum of the two results is used as the homogeneous reaction rate.

Laminar Finite-Rate Model-The laminar finite-rate model computes the chemical source terms using Arrhenius expressions and ignores the effects of turbulent fluctuations. The net source of chemical species i due to reaction R_i (kg/m^3-s) is computed as the sum of the Arrhenius reaction

sources over the N_R reactions that the species participate in, and is given as

$$R_i = M_{w,i}\sum_{r=1}^{N_R}\hat{R}_{i,r} \quad (15)$$

where $M_{w,i}$ is the molecular weight of species i and $R_{i,r}$ is the Arrhenius molar rate of creation/destruction of species i in reaction r.

The molar reaction of creation/destruction of species i in reaction r, which is $\hat{R}_{i,r}$ (kgmol/m^3-s) in Eq. (15), is given as

$$\hat{R}_{i,r} = \Gamma\left(\upsilon''_{i,r} - \upsilon'_{i,r}\right)\left(k_{f,r}\prod_{j=1}^{N_r}\left[C_{j,r}\right]^{\eta'_{j,r}} - k_{b,r}\prod_{j=1}^{N_r}\left[C_{j,r}\right]^{\eta''_{j,r}}\right) \quad (16)$$

where

N_r = number of chemical species in reaction r

$C_{j,r}$ = molar concentration of each reactant and product species j in reaction r (kgmol/m^3)

$\eta'_{j,r}$ = forward rate exponent for each reactant and product species j in reaction r

$\eta''_{j,r}$ = backward rate exponent for each reactant and product species j in reaction r.

The forward rate constant for reaction r, $k_{f,r}$, is computed using the Arrhenius expression

$$k_{f,r} = A_r T^{\beta} e^{-E_r/RT} \quad (17)$$

where

A_r = pre-exponential factor (consistent unit)

r = temperature exponent (dimensionless)

E_r = activation energy for the reaction (J/kgmol)

R = universal gas constant (J/kgmol-K).

If the reaction is reversible, the backward rate constant, $k_{b,r}$, is computed from the forward rate constant using relation below

$$k_{b,r} = \frac{k_{f,r}}{K_r} \quad (18)$$

where K_r is the equilibrium constant for the r-th computed from

$$K_r = \exp\left(\frac{\Delta S_r^0}{R} - \frac{\Delta H_r^0}{RT}\right)\left(\frac{p_{atm}}{RT}\right)^{\sum_{r=1}^{N_R}\left(\upsilon''_{j,r} - \upsilon'_{j,r}\right)} \quad (19)$$

where p_{atm} is the atmospheric pressure (101,325 Pa). The term within the exponential function represents the change in Gibbs free energy, and its components are computed as

$$\frac{\Delta S_r^0}{R} = \sum_{i=1}^{N}\left(\upsilon''_{i,r} - \upsilon'_{i,r}\right)\frac{S_i^0}{R} \quad (20)$$

$$\frac{\Delta H_r^0}{RT} = \sum_{i=1}^{N}\left(\upsilon''_{i,r} - \upsilon'_{i,r}\right)\frac{h_i^0}{R} \quad (21)$$

where S_i^0 and h_i^0 are the standard-state entropy and standard-state enthalpy (heat of formation), respectively.

Eddy Dissipation Model-The eddy-dissipation model which accounts for turbulence-chemistry interaction was described in Magnussen [12]. The overall rate of reaction for the fastest burning fuels is controlled by turbulent mixing. The net rate of production of species i due to reaction r, $R_{i,r}$, is given by the smaller of the two given expressions below:

$$R_{i,r} = \nu'_{i,r} M_{w,i} A \rho \frac{\varepsilon}{\kappa} \min_R\left(\frac{Y_R}{\nu'_{R,r} M_{w,R}}\right) \quad (22)$$

$$R_{i,r} = \nu'_{i,r} M_{w,i} AB \rho \frac{\varepsilon}{\kappa}\frac{\sum_P Y_P}{\sum_j^N \nu''_{j,r} M_{w,j}} \quad (23)$$

where

Y_P is the mass fraction of any product species, P

Y_R is the mass fraction of a particular reactant, R

A is an empirical constant equal to 4.0

B is an empirical constant equal to 0.5

$\nu'_{i,r}$ is the stoichiometric coefficient for reactant i in reaction r

$\nu''_{j,r}$ is the stoichiometric coefficient for product j in reaction r

In the above Eqs. (22) and (23), the chemical reaction rate is governed by the large-eddy mixing time scale, κ/ε, and an ignition source is not required. This is based on the assumption that the chemical reaction is much faster than the turbulence mixing time scale, so the actual chemical reaction is not important.

The reason for taking the minimum reaction rate calculated from the eddy-dissipation model and finite rate model is that, the Arrhenius rate is usually very slow at low temperatures and grows exponentially as the temperature increases, thus acting as a kinetic "switch"; once the flame is ignited and temperature becomes higher, the Arrhenius rate is much faster than the eddy-dissipation rate making the reactions mixing-limited.

In this study, the complete homogeneous reactions are:

$$CH_{3.086}O_{0.131} + 1.706\ O_2 \rightarrow CO_2 + 1.543\ H_2O \quad (24)$$

$$2\ CO + O_2 \rightarrow 2\ CO_2 \quad (25)$$

where in Eq. (25) CO comes from the following two-step carbon particle surface reactions:

$$C + CO2 \rightarrow 2CO$$

$$C + 0.5O2 \rightarrow CO$$

which are modeled as the heterogeneous reactions described below.

Heterogeneous reaction

The particle reaction, R (kg/m^2-s), is expressed as

$$R = D_0(C_g - C_s) = R_c(C_s)^N \quad (26)$$

Where

D_0 = bulk diffusion coefficient (m/s)

C_g = mean reacting gas species concentration in the bulk (kg/m^3)

C_s = mean reacting gas species concentration at the particle surface (kg/m^3)

R_c = chemical reaction rate coefficient (units vary)

N = apparent reaction order (dimensionless).

The concentration at the particle surface, C_s, is not known, so it is eliminated and the expression is recast as follows,

$$R = R_c\left[C_g - \frac{R}{D_0}\right]^N . \quad (27)$$

This equation has to be solved by an iterative procedure, with the exception of the cases when N = 1 or N = 0. When N = 1, Eq. (27) can be written as

$$R = \frac{C_g R_c D_0}{D_0 + R_c} . \quad (28)$$

In the cases of N = 0, if there is a finite concentration of reactant at the particle surface, the solid depletion rate is equal to the chemical reaction rate. If there is no reactant at the surface, the solid depletion rate changes abruptly to the diffusion-controlled rate.

$D_{o,r}$ is given by

$$D_{0,r} = C_{1,r}\frac{\left[\left(T_p + T_\infty\right)/2\right]^{0.75}}{d_p} . \quad (29)$$

In this study, two heterogeneous reactions are modeled and their reaction rates are:

1. C + 0.5O2 → CO

Rate coefficient: R = T(A+BT)
where A = -0.067 kmol/(m^2-s-K)
B = 5.26x10^{-5} kmol/m^2-s-K^2.

The reaction rate is based on the work of Field [13].

2. C + CO2 → 2CO

Rate coefficient: R = AT^nExp(-E/RT)
where n = 1.0
A = -4.4 kmol/m^2-s-K
E = 1.62 x 10^{+8} J/kmol.

The reaction rate is based on the work of Mayers [14]

In this study, the combustion of volatiles and gasified carbon is modeled by a single-step reaction. The mixing and transport of chemical species is modeled by solving the conservation equations describing convection, diffusion, and reaction sources for each component species. The species transport equations are solved by predicting the local mass fraction of each species, Y_i, through the solution of a convection-diffusion equation for the i-th species.

Grid and Meshes

The grid used in this study is generated using GAMBIT (version 2.2.30). Structured grids are employed in meshing the kiln, part of the main chamber, and the outlet duct. Unstructured grids are employed for all the other parts, namely the settling chamber, inlet duct, and part of the main chamber. All together there are 70,729 nodes, 708,418 faces and 340,800 cells. Meshes of each part are shown in detail in Fig. 4.

Grid sensitivity study

A grid sensitivity study of two different mesh numbers (325,431 and 968,235) has been performed and investigated. The computational time for the low mesh number case is about 20 hours and for the high mesh number case is about 60 hours in a parallel-processed 10-node cluster. The temperature variation within the whole domain lies within 50K to 150K (2.6%-7.9%). At the exit, the difference of mass-weighted temperature is about 90K (4.7%).

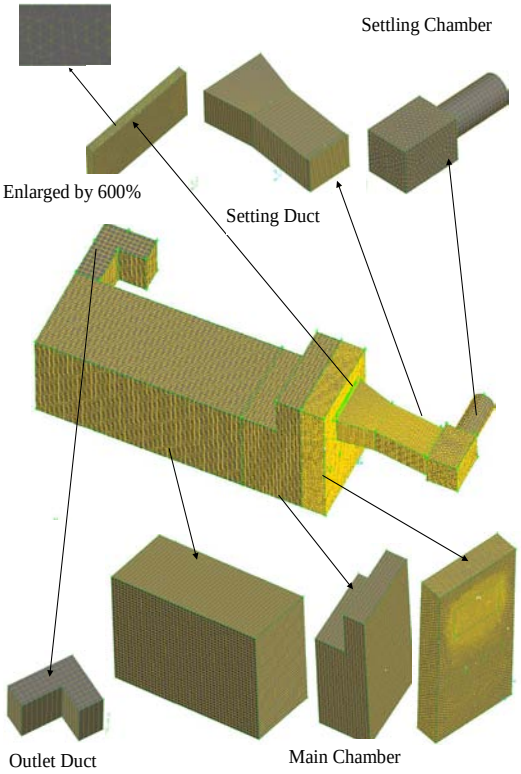

Fig.4 Meshes of different parts of the pyroscrubber

RESULTS AND DISCUSSION

Particle Combustion Model with 100% Stoichiometric Air

The simulation of combustion and thermal flow inside the pyroscrubber is conducted with the heterogeneous reaction model between solid carbon particle and gas implemented. Particle trajectory and mass change due to diffusion and combustion have been tracked to provide detailed information of particle reaction and flow behavior.

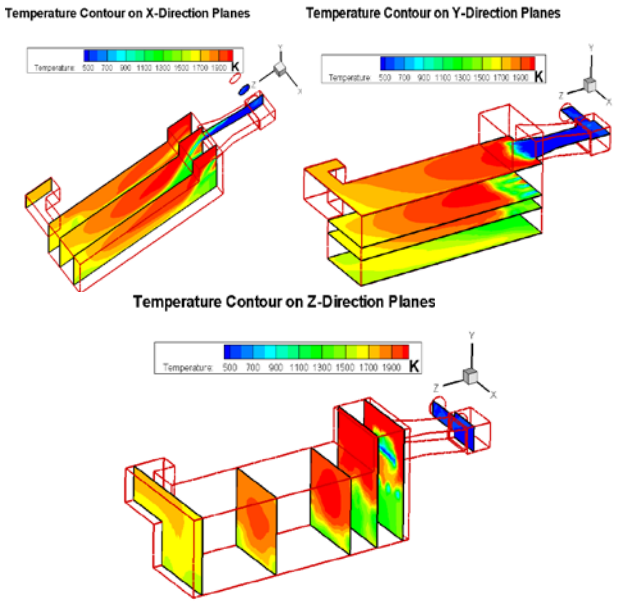

Coke particle combustion (100% stoichiometric air)

Fig. 5 Temperature contour inside the pyroscrubber on different planes for coke particle combustion with 100% stoichiometric air.

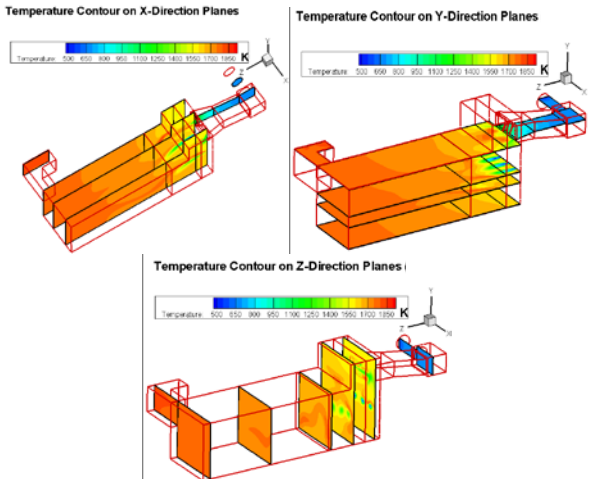

LHF Model Case (100% stoichiometric air)

Fig. 6 Temperature contours inside the pyroscrubber at different planes for the LHF model case (100% stoichiometric air) from Zhao and Wang[4]

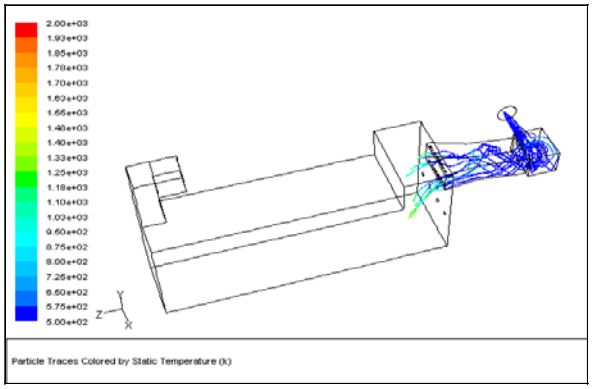

Fig. 7 Particle pathlines for coke particle combustion (100% stoichiometric air) showing particles are almost completely consumed in the high-bay area.

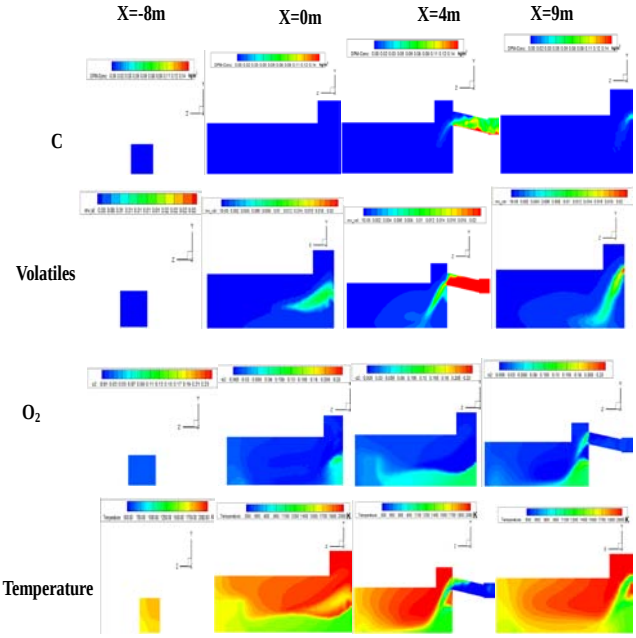

Coke particle combustion (100% stoichiometric air)

Fig. 8 Species and temperature contour plots on X-direction planes for coke particle combustion case (100% stoichiometric air).

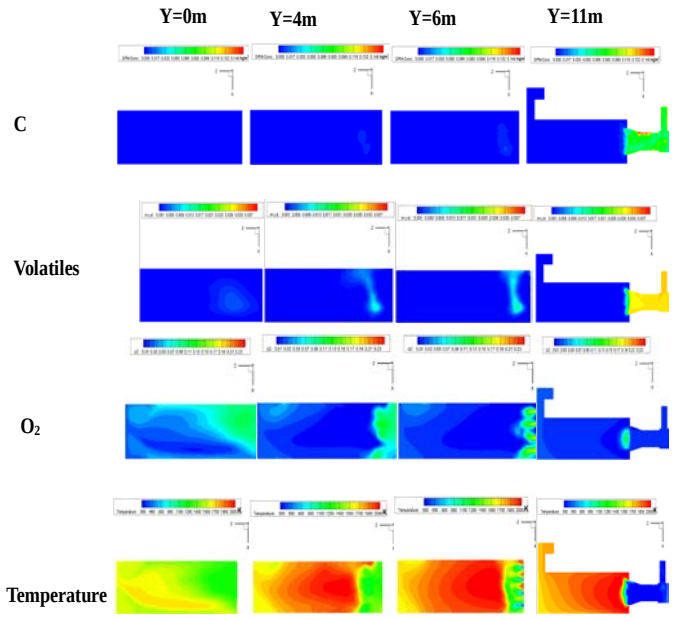

Coke particle combustion (100% stoichiometric air)

Fig. 9 Species and temperature contour plots on Y-direction planes for coke particle combustion case (100% stoichiometric air).

.

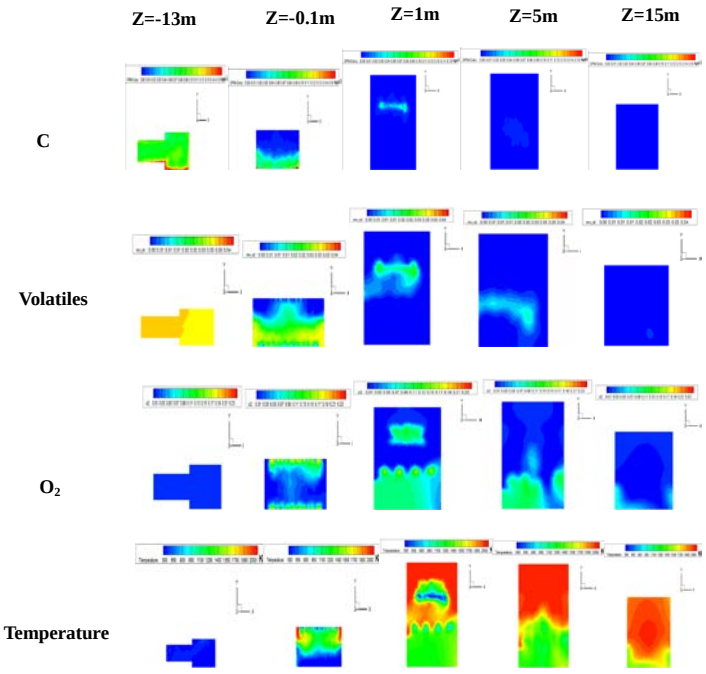

Coke particle combustion (100% stoichiometric air)

Fig. 10 Species and temperature contour plots on Z-direction planes for coke particle combustion case (100% stoichiometric air).

Temperature contours on different planes are shown in Fig. 5. For comparison, temperature contours from the case of LHF model with 100% stoichiometric air are shown in Fig. 6. Figure 7 shows some typical particle pathlines of particle combustion model and integral results are shown in Table 2. Exergy from the outflow is also shown in the Table 2, where evergy defined as $B=Q\ (1-T_o/T_{exit})$ is the maximal possible conversion of heat to work or "useful energy". T_{exit} is the temperature at the pyroscrubber exit and T_o is the temperature level at which the reject heat can be disposed, that is the temperature of the surrounding. The results are compared with the plant measurement data and the LHF model results of both the 100% and 150% stoichiometric air cases at three locations: center of the high bay ($\mathbf{T_1}$), center of the main chamber ($\mathbf{T_2}$), and center of the exit duct ($\mathbf{T_3}$). The results are summarized in Table 3. The following observations and analysis are made:

- The plant measurement temperature at the exit is 1,533K (2,791^{o}F). The mass-weighted average exit temperature from the simulation is 1,717K (3,122 ^{o}F) which is 184K (12%) higher. Considering the complexity of the model, the difference is reasonable. Also note that the simulation assumes the adiabatic wall condition, it is reasonable to interpret that the relatively lower measured temperature is partially attributed to heat losses through the walls in the real environment. The plant operators also report that they often provide 5-10% more air than stoichiometric value to ensure more complete combustion in most part of the pyroscrubber. The excessive air, therefore, also contributes to reduced temperature.
- LHF model with 100% stoichiometric air predicts the temperature in the high-bay area very well (around 2% based on the scale of temperature difference of plant measurement data and the pyroscrubber inlet temperature, $T-T_i$), but the temperature is over predicted at the exit. On the other hand, for the 150% stoichiometric air case, the predicted temperature value is very close to the measurement data at the exit (<1%) but under-predicts the temperature in the high bay. Considering that the high-bay area is where intensive combustion took place and in this area excess air from the low bay blowers has not been well mixed with the fuel yet, thus 100% stoichiometric air case well captures the combustion behavior in this region.

In the same manner, 150% air case under-predicts the high bay combustion temperature due to the over-excess air but captures the exit temperature better since the plant usually runs with up to 10% of excess air. To make it more evident, some numbers will be given. Assume the total air is equally supplied from the high-bay injection tubes and low bay blowers. So for 100% stoichiometric simulation case, 50% and 50% air is supplied from the high bay and low bay respectively, and 75% and 75% for 150% case. Assume 110% air is supplied under real running conditions, making it 55% and 55% from high bay and low bay respectively. Apparently 100% simulation case is close to the real running condition in

the high-bay combustion zone (50% and 55%) and 150% case over-cooled this area (75% and 55%). At the exit 100% case over predicts the temperature comparing with the real case with excess air. The 150% case supposedly will under-predict temperature at the exit but the adiabatic wall condition offsets the effect of excess air making the temperature close to the measurement.

- An interesting observation shows that quite different from the LHF model results, in which the temperatures inside the chamber (T_1 and T_2) are lower than the exit temperature (T_3), the temperature changing trend of the particle combustion model is consistent with the real measurement data, i.e. temperature is lower at the exit. And the temperatures from the particle combustion model are consistently higher than the measurement data by around 15%. Again this could be partly attributed to the perfectly insulated wall condition assumed in this study. The consistent temperature pattern tends to suggest that the particle combustion model better captures the temperature distribution inside the pyroscrubber than the LHF model.
- Particle combustion model generates much higher local flame temperature (2,200K, 3,992 ^{o}F) than LHF model (1,800K, 3,272 ^{o}F). This is probably partially caused by less gas volume flow surrounding the solid particles until they are completely consumed and become gaseous products. The high-temperature area of the particle combustion model occurs in the high-bay area; in contrast, the LHF model shows the high-temperature near the pyroscrubber exit.
- Particle pathlines in Fig. 7 shows that all coke particles are burned before or in the high-bay area, and coke particles are burned out very quickly once they enter the high-bay area.
- Intensive combustion and the highest temperature occur on the top part of the main chamber and close to the high-bay area. On the bottom of the chamber the gas temperature is 300 K lower than in the hot area. This is different from the LHF case of which the highest temperature occurs in the later part of the main chamber and is almost uniformly distributed across the vertical cross section of the main chamber.
- For both eddy dissipation model and the particle combustion model, the gas temperature is uniform in the area close to the outlet duct. But the outflow temperature of the particle combustion model is 100k lower than the LHF model case. Total energy of the particle combustion case is 92% of the LHF model case.
- Particle size affects its trajectory inside the pyroscrubber, affecting the combustion process. Particles larger than 200 μm in diameter can be easily trapped at the corners of the flue passage, especially in the front-facing walls between different chambers. Only approximately 10% of the particles larger than 200 μm can be transported into the main chamber. Most of the particles less than 20 μm can be successfully transported through the flue passage into the main chamber.

Table 2: Simulated results of particle combustion (100% stoichiometric air)

100% air(particle combustion)	main inlet mass flow rate(kg/s)	burner mass flow rate(kg/s)	air injection mass flow rate(kg/s)	outlet mass flow rate(kg/s)	outlet mass fraction
CO	0.00E+00	0.00E+00	0.00E+00	4.91E-08	1.33E-09(0.0015 ppm)
Volatiles	0.42	0.00	0.00	0.00	0.00E+00
O_2	0.24	2.66	2.53	0.92	2.49E-02
CO_2	2.16	0.00	0.00	8.63	2.34E-01
H_2O	1.15	0.00	0.00	1.84	4.98E-02
C(s)	1.53	0.00	0.00	0.00	0.00E+00
N_2	9.78	8.82	8.35	25.56	6.92E-01
total	14.58	11.48	10.88	36.94	1.02E+00
Exit Temp	1717K (3123^{o}F)	Exergy (Useful	52.20MW		

Table 3: Comparisons of the results of the particle combustion model with the measured data and the results of LHF model with 100% and 150% stoichioimetric air cases

	T_1 (K)	T_2 (K)	T_3 (K)
Measured Data	1616	1616	1533
LHF Model (100% air)	1641	1770	1804
Difference (LHF)	2.24%	13.80%	26.23%
LHF Model (150% air)	1508	1518	1523
Difference (LHF, 150%	-9.68%	-8.78%	-0.97%
Particle Model	1882	1869	1717
Difference (Particle, 100%)	23.84%	22.67%	17.81%

Bottom Doors Opening Cases

Motivated by the potential benefit of cutting e power consumption for air injection, bottom doors opening cases are investigated. In this case, ambient air is expected to be drafted into the pyroscrubber, thus offering the possibility of saving a portion of air-blowers' power. The locations of the bottom doors are shown in Fig. 11. Each door sizes at 10 ft x 10 ft. Since LHF can effectively simulate the overall thermal-flow behavior in the pyroscrubber and the save 90% of computational time in comparison with the solid particle combustion model, the LHF model is adopted for the bottom doors opening cases.

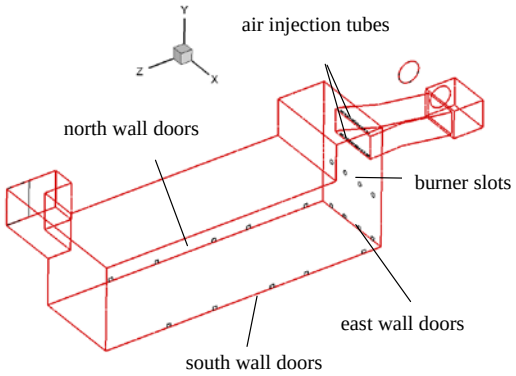

Fig. 11 Locations for bottom doors, air injections tubes, and burner slots.

Three cases are investigated with open bottom doors:

- Case 1 - All doors open plus 100% air. In this case, all the bottom doors are completely open, and the air is also blown in through injectors at 100% stoichiometric condition.
- Case 2 - Doors partially open plus 100% air. All doors on south and north walls are closed and only the doors on east wall are open. Air injection is at 100% stoichiometric condition.
- Case 3 - All doors open with no air injection. All the air injections from air injection tubes and burner slots are closed, while all the bottom doors are open.

Figure 12 shows the wall temperature contours of the three cases involving natural air draft. It is noticed for all three cases that a large amount of ambient air is entrained (sucked) into the chamber by the buoyancy force of the rising hot combusted gas. Combustion is clearly shown being restrained on the upper region of the main chamber. Bottom of the chamber is almost completely occupied with the cold air. Due to the large density difference between the hot gas and the cold air, the flow inside the main chamber is stably stratified without any visible large-scale mixing. The highest temperature of the three cases is about the same as the previous case without opening the doors at 1,800K. Cases 1 and 3 with all doors open reduce the high-temperature areas in comparison with the partially open case (Case 2). Simulation results of the three cases are shown in Table 4. The induced draft is entrained through the doors with a respectable momentum at an average velocity of 4 m/s (8.95 mph) with mass flow rate at 27.68 kg/s (219,725 lbm/hr), 9.72 kg/s (77,951 lbm/hr), and 32.29 kg/s (256,319 lbm/hr) for Cases 1, 2 and 3 respectively, which are approximately 190%, 67%, and 221% of the total mass flow rate from the pyroscrubber inlet.

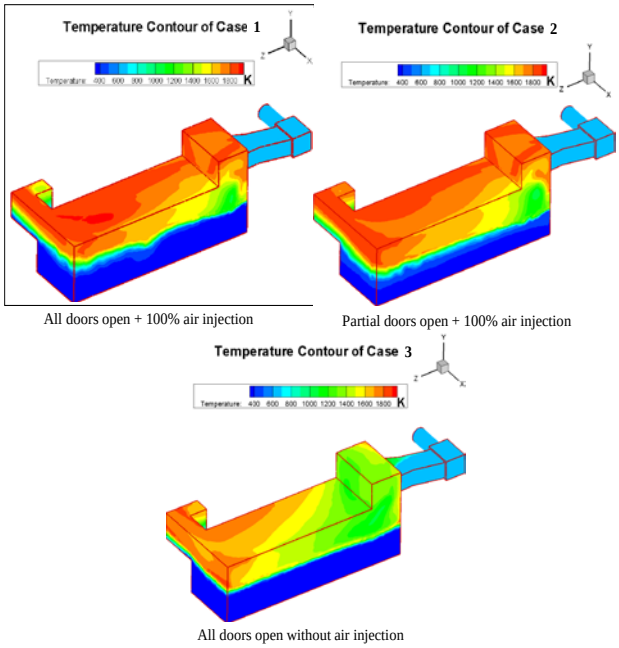

Fig. 12 Wall temperature contours in the pyroscrubber for three bottom doors opening case (Cases 1-3).

Table 4: Simulated results of three bottom door opening cases (Cases 1-3)

		mass flow(kg/s)	velocity(m/s)	temperature(K)	exergy (MW)
Case 1	inlet	14.58	4.19	500	-
(All doors open + 100% air injection)	air injection	10.88	14.35	300	-
	burner	11.48	10.15	300	-
	bottom doors	27.68	4.90	300	-
	outlet	64.62	11.58	1190	50.60
Case 2	inlet	14.58	4.19	500	-
(Doors partially open + 100% air)	air injection	10.88	14.35	300	-
	burner	11.48	10.15	300	-
	bottom doors	9.72	6.00	300	-
	outlet	46.66	11.15	1534	55.69
Case 3	inlet	14.58	4.19	-	-
(All doors open, no air)	air injection	0.00	0.00	-	-
	burner	0.00	0.00	-	-
	bottom doors	32.29	5.71	300	-
	outlet	46.86	11.15	1468	52.44

Case 1 with all doors open plus 100% air injection is apparently the worst case because the extra air entrained through the bottom doors only cools down the hot combustion gas (about 340 K temperature drop) and downgrades the exergy.

Closing all air injection and using only the entrained air through opening bottom doors for combustion in Case 3, although is not a controllable way of combustion, it is interesting to see that a comparable amount of air can be entrained as is in 100% air injection. The potential saving of blowers' power is 1.71 kW accompanied with a loss of exergy of 4.73 MW. The stratified flow pattern generates a much weaker mixing effect than using the air injection tubes and burner slots; as a result, combustion is not as complete as the 150% stoichiometric air combustion case studied in [4] and the temperature is lower.

Moreover, it is not convenient to control the induced air flow.

CONCLUSIONS

A computational study of combustion and thermal flow inside the pyroscrubber is conducted with a solid particle combustion model by incorporating both finite-rate heterogeneous and homogeneous combustion processes, which provides a more accurate modeling of the complex solid carbon particle surface reaction, heat transfer, and species transport. Particle trajectory and mass change due to diffusion and combustion have been tracked to provide detailed information of particle reaction and flow behavior. Results reveal that the particle combustion model generates much higher local flame temperature (2,200K) than the LHF model (1,800K) studied in [4]. All char particles are burned before or in the high-bay area, and char particles burn out very quickly once they enter the high-bay area. Total exergy output of the case with particle combustion model is 92% of the LHF model case with 100% stoichiometric air.

Furthermore, this study further investigates the possible benefit of running the pyroscrubber with the ventilation doors on the bottom open. Three cases with different combinations of air injections and door opening portions have been studied. Results show that the gas flow is stably stratified with a large amount of the entrained cold air moving at the bottom of the chamber and hot combusted gases moving through the top. Running with all doors open plus 100% air injection is the worst case due to the cooling effect of the excess air (about 340 K temperature drop) and the downgraded exergy. With bottom doors completely open, sufficient air will be drawn into the pyroscrubber giving the possibility of energy saving by cutting blowers power supply, but the advantage of saving the blower power is not as critical as keeping the combusted gases at higher temperatures. Furthermore, one major concern on employing naturally aspirated method is that the drafted air flow is hard to control so the pyroscrubber performance could be compromised by producing less exergy.

ACKNOWLEDGEMENTS

This study was supported by Rain CII Carbon, LLC. Part of the funding was provided by the Louisiana Board of Regents' Industrial Ties Research Subprogram.

REFERENCES

[1] Bagdoyan, E. A., and Gootzait, E., “Refiners Calcine Coke,” Hydrocarbon Processing, September 1985, pp.85-90.

[2] Lee J. M., Baker J. J., Rolle J. G., Llerena R., “Characterization of Green and Calcined Coke Properties Used For Aluminum Anode-grade Carbon,” 217th ACS National Meeting, Dallas, Preprints of Symposia, Division of Fuel Chemistry, Vol. 43, No. 2 (1998).

[3] Byrne, Henry James, United States Patent 4,012,202, 1977.

[4] Zhao, L. and Wang, T., "Simulation of Combustion and Thermal-flow Inside a Pyroscrubber," Proceedings of IMECE2009, November 2009.

[5] Zhang, Z. and Wang, T., "Simulation of Combustion and Thermal-flow Inside a Petroleum Rotary Calcining Kiln, Part 1: Process Review and Modeling, " Proceedings of IMECE2009, November 2009.

[6] Zhang, Z. and Wang, T., "Simulation of Combustion and Thermal-flow Inside a Petroleum Rotary Calcining Kiln, Part 2: Analysis of Effects of Tertiary Airflow and Rotation, " Proceedings of IMECE2009, November 2009.

[7] Ranz, W. E. and Marshall, W. R. Jr., 1952, “Evaporation from Drops, Part I,” Chem. Eng. Prog., 48, pp. 141-146.

[8] Ranz, W. E. and Marshall, W. R. Jr., 1952, “Evaporation from Drops, Part II,” Chem. Eng. Prog., 48, pp. 173-180.

[9] Kuo, K. Y., 1986, Principles of Combustion, John Wiley and Sons, New York.

[10] Baulch, D. L., Drysdall, D. D. and Lloyd, L. C., “Evaluated Kinetic Data for High Temperature Reactions,” Butterworth, volume 1,2,3. 1973.

[11] Fluent 6.3 User’s Guide, September 2006, Fluent Inc.

[12] Magnussen, B. F. and Hjertager, B. H. “On mathematical models of turbulent combustion with special emphasis on soot formation and combustion,” 16th Symp (Int'l) on Combustion, The Combustion Institute, 1976.

[13] Field, M.A., “Rate of Combustion of Size-Graded Fractions of Char From a Low-Rank Between 1200 K and 2000 K,” Combustion and Flame 13, 237, 1968.

[14] Mayers, M.A., “The Rate Reduction of Carbon Dioxide by Graphite,” Journal of American Chemical Society 56, 70, 1934.